Journal of Sound and Vibration (1998) **217**(5), 883–907
Article No. sv981801

FLUID DAMPING CONTROLLED INSTABILITY OF TUBES IN CROSSFLOW

S. S. Chen and Y. Cai

Energy Technology Division, *Argonne National Laboratory*, *Argonne*, *IL*, *U.S.A.*

and

G. S. Srikantiah

Nuclear Power Division, *Electric Power Research Institute*, *Palo Alto*, *CA*, *U.S.A.*

(*Received* 23 *June* 1997, *and in final form* 15 *June* 1998)

The mathematical model for fluid damping controlled instability of tubes in crossflow presented in this paper is based on unsteady flow theory. Motion-dependent fluid forces are measured in a water channel. From the measured fluid forces, fluid stiffness and fluid damping coefficients are calculated as a function of reduced flow velocity, oscillation amplitude, and Reynolds number. Once these coefficients are known, the mathematical model can be applied to predict structural instability due to fluid damping. The cases considered are a single tube, twin tubes, tube row, triangular array, and square arrays. The results show instability regions that are based on the fluid damping coefficients and provide answers to a series of questions on fluidelastic instability of tube arrays in crossflow.

1. INTRODUCTION

Several theories have been used to study the vibration and stability of tubes in crossflow: quasistatic, quasisteady, and unsteady flow theoreis [1–3]. In some parameter ranges, both quasistatic and quasisteady flow theories have certain advantages because they provide a simple way to obtain motion-dependent fluid forces. However, only the unsteady flow theory can be applied in any range of parameters. In this study, unsteady flow theory is used.

Can fluidelastic instability occur for a flexible tube in a rigid tube array subjected to crossflow? It is a frequently asked question. In the original stability criterion developed by Connors [4], at least two flexible tubes are needed to attain fluidelastic instability. In the case considered by Connors, the instability was due to fluid stiffness controlled instability and a minimum of two degrees of freedom were needed. Tests by various experimentalists found that a single flexible tube in a tube array shows instability in some cases, whereas, in other cases, it is stable [5–7]. Chen [5, 8] developed a mathematical model based on the measured motion dependent fluid forces of Tanaka and his colleagues [9–11] to characterize the difference between the two mechanisms that provide the theoretical basis for the

0022–460X/98/450883 + 25 $30.00/0

occurrence of different stability mechansims. In the past, because the amount of available fluid force coefficient data was limited, the theory could not provide quantitative answers about the stability of tubes in various situations.

Recently, extensive tests of motion dependent fluid forces have been performed [12–16]. The unsteady fluid forces and unsteady flow theory will provide answers to some frequently asked questions on fluidelastic instability. The purpose of this paper is to study fluid damping controlled instability of tubes in differing situations.

2. UNSTEADY FLOW THEORY

Consider a tube oscillating in crossflow as shown in Figure 1. The tube may stand alone or be surrounded by other rigid tubes. The fluid is flowing at velocity U. When the tube is stationary, it is subjected to drag and lift forces. The displacement components of the tube in the x and y directions are u and v, respectively. Once the tube starts to move, additional fluid forces, called motion dependent fluid forces, are induced because of the tube motion. The motion dependent fluid force components per unit length that act on the tube in the x and y directions are f and g, respectively, and are given [1, 2] as

$$f = -\rho\pi R^2\left(\alpha\frac{\partial^2 u}{\partial t^2} + \sigma\frac{\partial^2 v}{\partial t^2}\right) + \frac{\rho U^2}{\omega}\left(\alpha'\frac{\partial u}{\partial t} + \sigma'\frac{\partial v}{\partial t}\right) + \rho U^2(\alpha'' u + \sigma'' v), \quad (1)$$

and

$$g = -\rho\pi R^2\left(\tau\frac{\partial^2 u}{\partial t^2} + \beta\frac{\partial^2 v}{\partial t^2}\right) + \frac{\rho U^2}{\omega}\left(\tau'\frac{\partial u}{\partial t} + \beta'\frac{\partial v}{\partial t}\right) + \rho U^2(\tau'' u + \beta'' v), \quad (2)$$

where ρ is fluid density; R is tube radius; t is time; ω is circular frequency of the tube oscillations; α, β, σ, and τ are added-mass coefficients; α', β', σ', and τ' are fluid damping coefficients; and α'', β'', σ'', and τ'' are fluid stiffness coefficients.

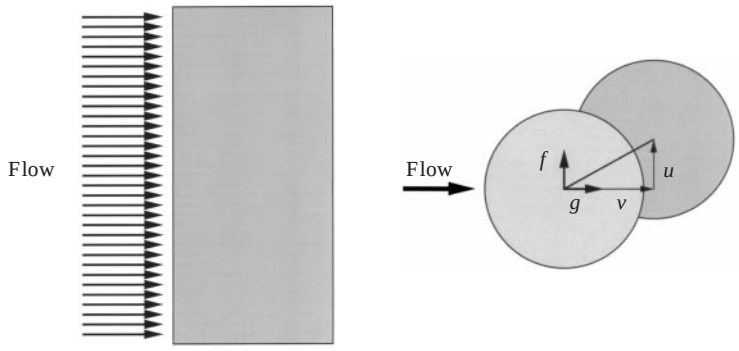

Figure 1. Tube oscillating in crossflow.

Various methods can be used to determine fluid force coefficients. In this study, unsteady flow theory has been used. Fluid force coefficients can be determined by measuring the fluid forces acting on the tube as a result of its oscillations. If the tube is excited in the x direction, its displacement in the x direction is given by

$$u = d_0 \cos \omega t, \tag{3}$$

where d_0 is the oscillation amplitude. The motion dependent fluid force components acting on the tube in the x and y directions are

$$f = \tfrac{1}{2}\rho U^2 e_l \cos(\omega t + \phi_l) d_0 \tag{4}$$

and

$$g = \tfrac{1}{2}\rho U^2 e_d \cos(\omega t + \phi_d) d_0, \tag{5}$$

where e_l and e_d are the fluid force amplitudes and ϕ_l and ϕ_d are the phase angles by which the fluid forces acting on the tube lead the displacement of the tube.

By using equations 1–3, one can also write the fluid-force components as

$$f = (\rho\pi R^2\omega^2\alpha + \rho U^2\alpha'')d_0 \cos \omega t - \rho U^2\alpha' d_0 \sin \omega t, \tag{6}$$

and

$$g = (\rho\pi R^2\omega^2\tau + \rho U^2\tau'')d_0 \cos \omega t - \rho U^2\tau' d_0 \sin \omega t. \tag{7}$$

Solving equations 4 and 6 and equations 5 and 7, one obtains

$$\alpha'' = \tfrac{1}{2}e_l \cos \phi_l - (\pi^3/Ur^2)\alpha, \qquad \tau'' = \tfrac{1}{2}e_d \cos \phi_d - (\pi^3/Ur^2)\tau,$$
$$\alpha' = \tfrac{1}{2}e_l \sin \phi_l, \qquad \tau' = \tfrac{1}{2}e_d \sin \phi_d, \tag{8}$$

where Ur is the reduced flow velocity ($Ur = \pi U/\omega R$). The added-mass coefficients α and τ can be calculated from the potential flow theory [1]; they can also be measured from the excitation of the tube in stationary fluid. Other fluid force coefficients, β', β'', σ', and σ'' can be obtained in a similar manner by exciting the tube in the y direction.

3. MOTION DEPENDENT FLUID FORCE COEFFICIENTS

3.1. EXPERIMENTAL SETUP AND PROTOCOL

A water channel was used to measure motion dependent fluid forces. The test setup and measurement technique were presented in an earlier paper [12]. Many cases were considered in this study (Figure 2). Various tube arrays are described by the tube pitch in the drag direction P, the lift direction T, and tube diameter D ($D = 2{\cdot}54$ cm).

Case a—single tube: the tube was located in the middle of the water channel (Figure 2(a)). Flow velocities of 0·064, 0·11 and 0·127 m/s were tested. The tube was excited to various oscillation amplitudes in the lift direction.

Case b—two tubes normal to flow (Figure 2(b)): $T/D = 1{\cdot}35$. Flow velocities of 0·05, 0·07, 0·113, 0·146 and 0·166 m/s were tested. The tube was excited in the lift and drag directions.

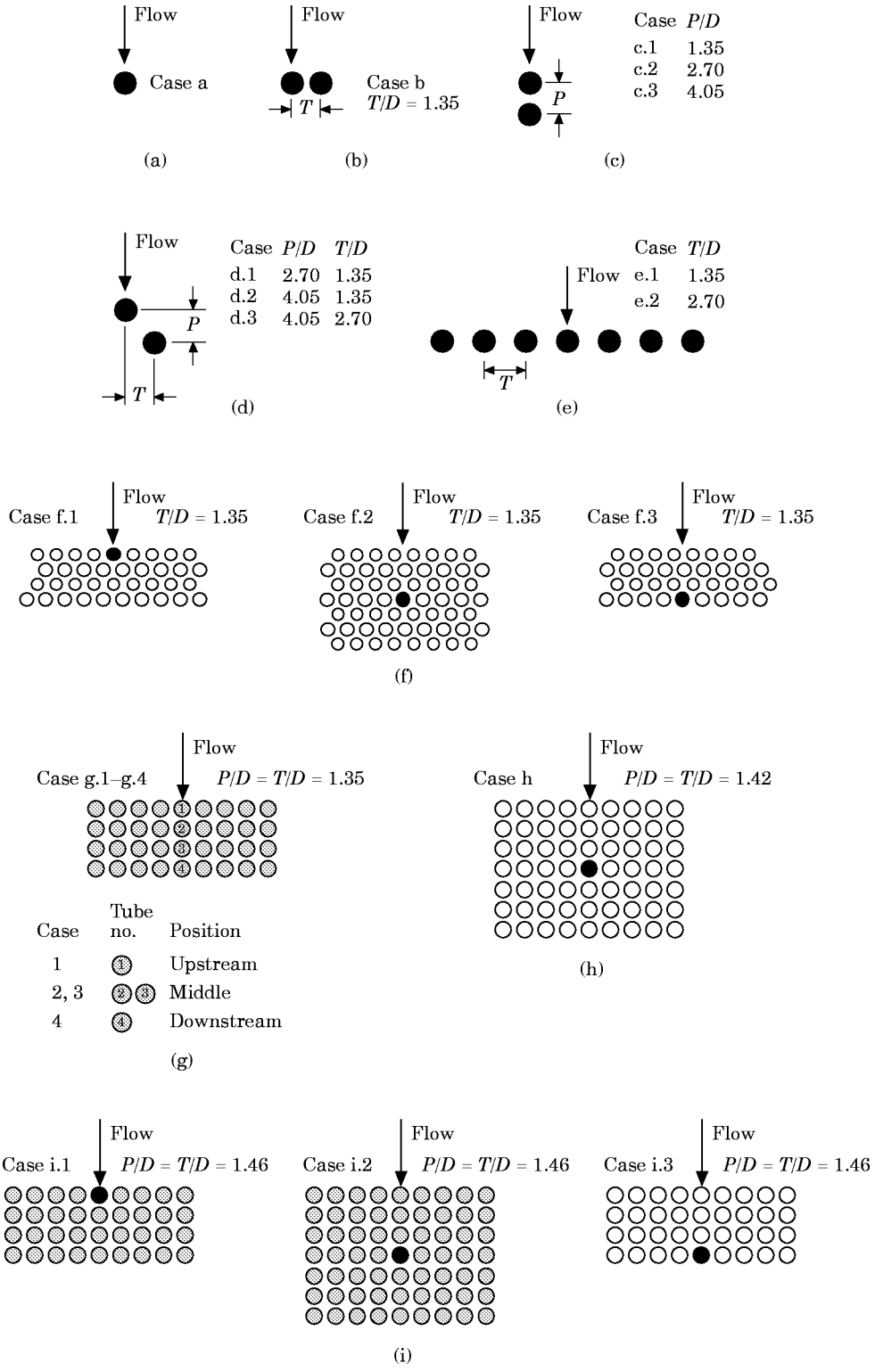

Figure 2. Tube arrays in crossflow studied in this investigation: (a) single tube; (b) two tubes normal to flow; (c) two tubes in tandem; (d) tube in the wake of another tube; (e) tube row; (f) triangular arrays ($T/D = 1{\cdot}35$); and (g, h, i) square arrays: $P/D = T/D = 1{\cdot}35$ (tube positions; (h) 1·42, (i) 1·46).

Cases c.1–c.3—two tubes in tandem (Figure 2(c)): $P/D = 1{\cdot}35$ (case c.1), 2·70 (case c.2) and 4·05 (case c.3). For case c.1, the tube in the upstream position was excited at flow velocities of 0·07, 0·11, and 0·15 m/s in the lift and drag directions. For the tube in the downstream position in cases c.1, c.2 and c.3 the flow velocity was set at 0·11 m/s and the excitation amplitude was set at various values.

Cases d.1–d.3—a tube in the wake of another rigid tube (Figure 2(d)): Three cases were tested: case d.1, $P/D = 2{\cdot}7$, $T/D = 1{\cdot}35$; case d.2, $P/D = 4{\cdot}05$, $T/D = 1{\cdot}35$; and case d.3, $P/D = 4{\cdot}05$, $T/D = 2{\cdot}70$. The flow velocity was set at 0·11 m/s and the excitation amplitude was set at various values.

Cases e.1 and e.2—tube row (Figure 2(e)): $T/D = 1{\cdot}35$ (case e.1) and 2·7 (case e.2). In case e.1, flow velocities were 0·063, 0·092, 0·125, and 0·131 m/s. In case e.2, the flow velocity was set at 0·11 m/s and the excitation amplitude was set at various values.

Cases f.1–f.3—triangular array: $T/D = 1{\cdot}35$: the tube was located in the upstream (case f.1), middle (case f.2), or downstream (case f.3) position in the tube array (Figure 2(f)). Tests were performed at $U = 0{\cdot}07$, 0·11, and 0·16 m/s.

Cases g.1–g.4—square array with $P/D = T/D = 1{\cdot}35$: the tube was located in the upstream (case g.1), middle (case g.2, case g.3), or downstream (case g.4) position in the tube array, corresponding to tubes 1, 2, 3, and 4 shown in Figure 2(g). Tests were performed at $U = 0{\cdot}1$ m/s and tests were repeated for each case.

Case h—square array with $P/D = T/D = 1{\cdot}42$: the tube was located in the middle of the tube array (Figure 2(h)). The flow velocities were set at 0·06, 0·11, and 0·16 m/s.

Case i.1–i.3—square array with $P/D = T/D = 1{\cdot}46$: the tube was located in the upstream (case i.1), middle (case i.2), or downstream (case i.3) position in the tube array (Figure 2(i)). Two flow velocities were tested for case i.1 ($U = 0{\cdot}11$ and 0·165 m/s) and case i.3 ($U = 0{\cdot}125$ and 0·18 m/s) and three flow velocities were tested for case c.2 ($U = 0{\cdot}06$, 0·11, and 0·16 m/s).

The flexible tube in various cases was excited in the lift (x) or drag (y) direction, with a displacement $u(t) = d_0 \cos \omega t$. The fluid forces acting on the tube $f(t)$ and $g(t)$ were measured simultaneously with the displacement. From the time histories of fluid forces, fluid damping coefficients α' and τ' and fluid stiffness coefficients α'' and τ'' were calculated from equations 8; similar equations were used to calculate β', σ', β'' and σ'' in the drag direction.

Fluid force coefficients are a function of flow velocity, excitation frequency and excitation amplitude. In each case, when the flow velocity is set at a specific value, the tube is excited at a frequency of 0.2–2·0 Hz with a series of amplitudes d(0·6–3·5 mm), where d is the R.M.S. value of $u(t)$, given in equation 3. Reynolds number (Re) varied from $\approx$1500–4500, depending on the gap velocity U.

3.2. RESULTS

Figures 3–15 show the experimentally determined fluid force coefficients, all of which were plotted as a function of reduced flow velocity Ur ($= U/fD$; U = gap velocity, $f = \omega/2\pi$, D = tube diameter). Extensive data are presented in this paper.

The purposes are to provide the needed information in mathematical models and evaluations of analytical and numerical results, and to show the changes of characteristics in various tube arrays. The following general characteristics of the fluid force coefficients were observed:

(1) At high reduced flow velocity, the coefficients were almost independent of reduced flow velocity and excitation amplitude. This characteristic is similar for all tube arrays and other geometries [2]. Therefore, at high reduced flow velocity, the fluid force coefficients are much easier to quantify. Once, the coefficients are determined for a specific set of parameters, they can be applied to various values of flow velocity, excitation frequency, and excitation amplitude.

(2) Drastic changes in the fluid force coefficients occurred in the region of low reduced flow velocity ($Ur < 10$).

(3) In the critical region that corresponds to the lower reduced flow velocity, the magnitude of the coefficients also depends on the excitation amplitude.

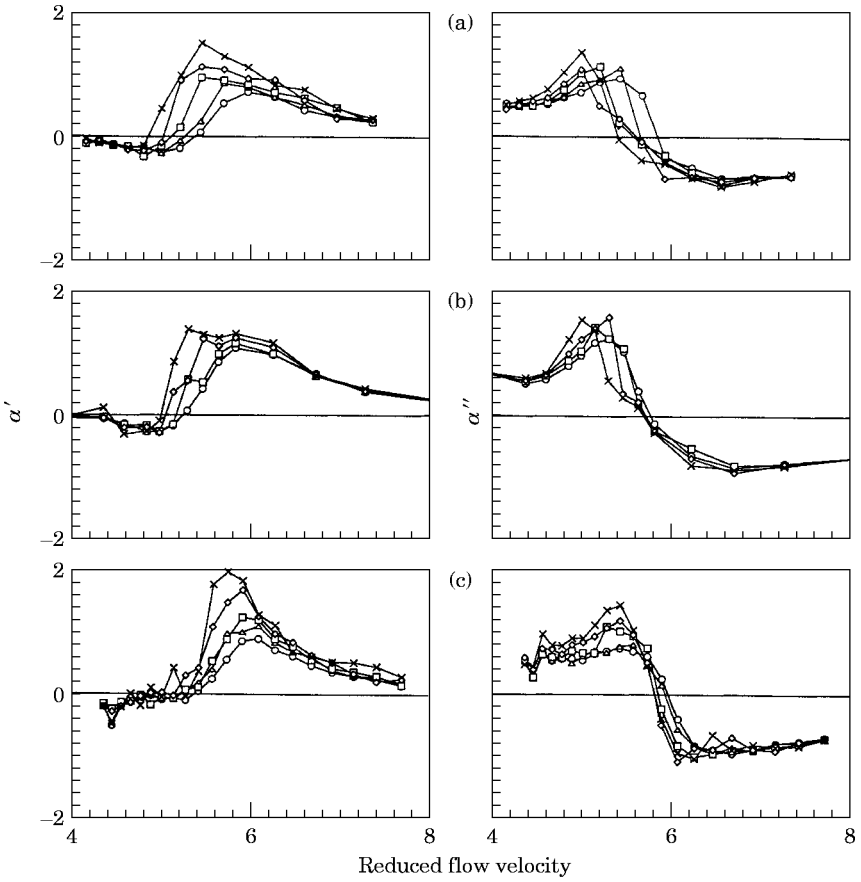

Figure 3. Fluid damping coefficient α' and fluid stiffness coefficient α'' for a single tube (case a) for three Reynolds numbers: (a) Re = 1610; –○–, d = 4 mm; –△–, d = 3·3 mm; –□–, d = 2·6 mm; –◇–, d = 1·9 mm; –×–, d = 1·2 mm; (b) Re = 2760; –○–, d = 2·4 mm; –□–, d = 2 mm; –◇–, d = 1·6 mm; –×–, d = 1·2 mm; (c) Re = 3190, –○–, d = 3·6 mm; –△–, d = 3 mm; –□–, d = 2·4 mm; –◇–, d = 1·8 mm; –×–, d = 1·2 mm.

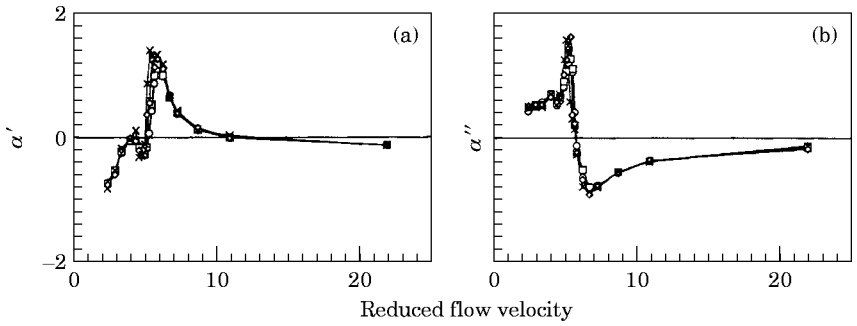

Figure 4. (a) Fluid damping coefficient α' and (b) fluid-stiffness coefficient α'' for a single tube (case a) for Re = 2760: –○–, d = 2·4 mm; –□–, d = 2 mm; –◇–, d = 1·6 mm; –×–, d = 1·2 mm.

The following additional characteristics were noted for each of the cases that were studied.

3.2.1. *Single tube*

From Figures 3 and 4 and from additional data not included here, α' is positive for *Ur* from ≈5–11, and its value decreases with excitation amplitude. The range depends on Re and oscillation amplitude.

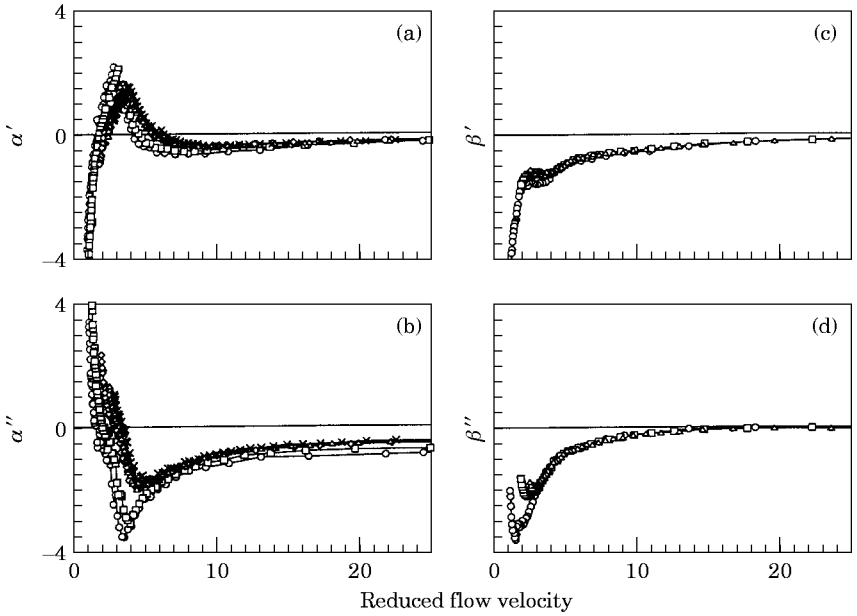

Figure 5. (a) Fluid damping coefficient α', (b) fluid stiffness coefficient α'', (c) fluid damping coefficient β' and (d) fluid stiffness coefficient β'' for two tubes normal to flow (case b). (a, b) –○–, Re = 1250; –□–, Re = 1760; –◇–, Re = 2830; –△–, Re = 3660; –×–, Re = 4160. (c, d) –○–, Re = 1760; –□–, Re = 2840; –△–, Re = 3870.

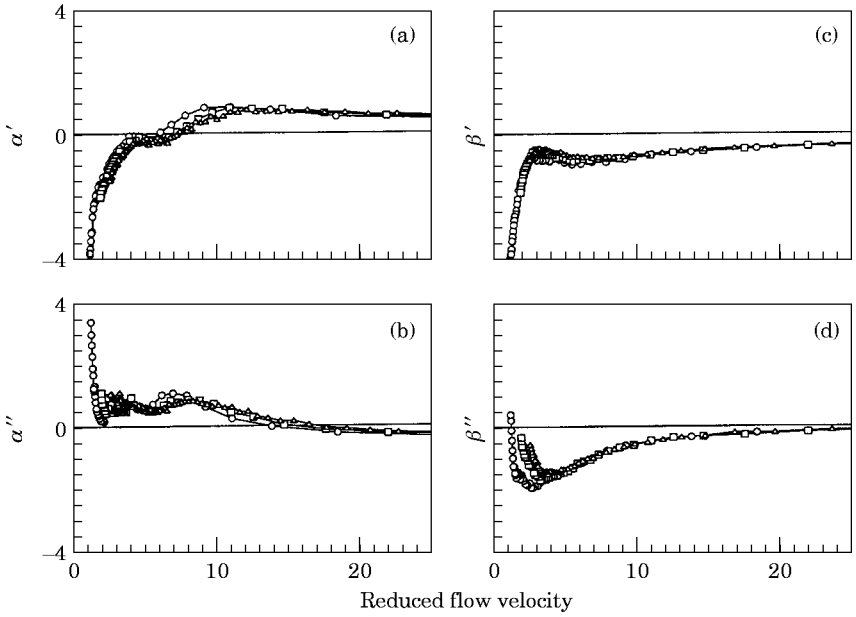

Figure 6. (a) Fluid damping coefficient α', (b) fluid stiffness coefficient α'', (c) fluid damping coefficient β' and (d) fluid stiffness coefficient β'' for tube in upstream position of two tubes in tandem (case c): −○−, Re = 1760; −□−, Re = 2760; −△−, Re = 3760.

At lower Re, α' becomes positive at lower Ur. At higher Re, α' becomes positive at higher Ur. However, its range varies from $\approx$4·8–5·4. As Ur is increased, α' becomes negative again.

At lower oscillation amplitudes, α' becomes positive at lower Ur; however, at higher oscillation amplitudes, it becomes positive at higher Ur. Moreover, the range of α' also depends on Re. As Ur is increased, the effect of oscillation amplitude is small.

The value of α'' is positive for smaller Ur and becomes negative as Ur is increased. The crossing point where the sign of α'' changes varies from Ur = 5·4–6·0. At high reduced flow velocity, both α' and α'' are approximately independent of Re, Ur and oscillation amplitude. The values of Ur that correspond to the peak values of α' and α'' increase with excitation amplitude and Re, and the peak values of α' and α'' are approximately the same for various values of Re.

3.2.2. *Two tubes normal to flow*

β' is negative throughout the whole range of Ur. α' is negative at lower Ur; its range depends on Re. A comparison of Figure 5 with Figure 3 reveals that the region for negative α' is at lower Ur for case b than for case a. As Re increases, the region of negative α' in case b shifts to higher Ur and its range increases slightly. However, the peak magnitude of α' decreases with Re. This is similar to the case of a single tube, as shown in Figure 3.

3.2.3. *Two tubes in tandem*

In case c.1, α' becomes positive as soon as Ur reaches a certain value, which is equal to 6–7 for the tube in the upstream position, Figure 6. The precise crossing point depends on Re and α' continues to be positive at high Ur (in this case, the

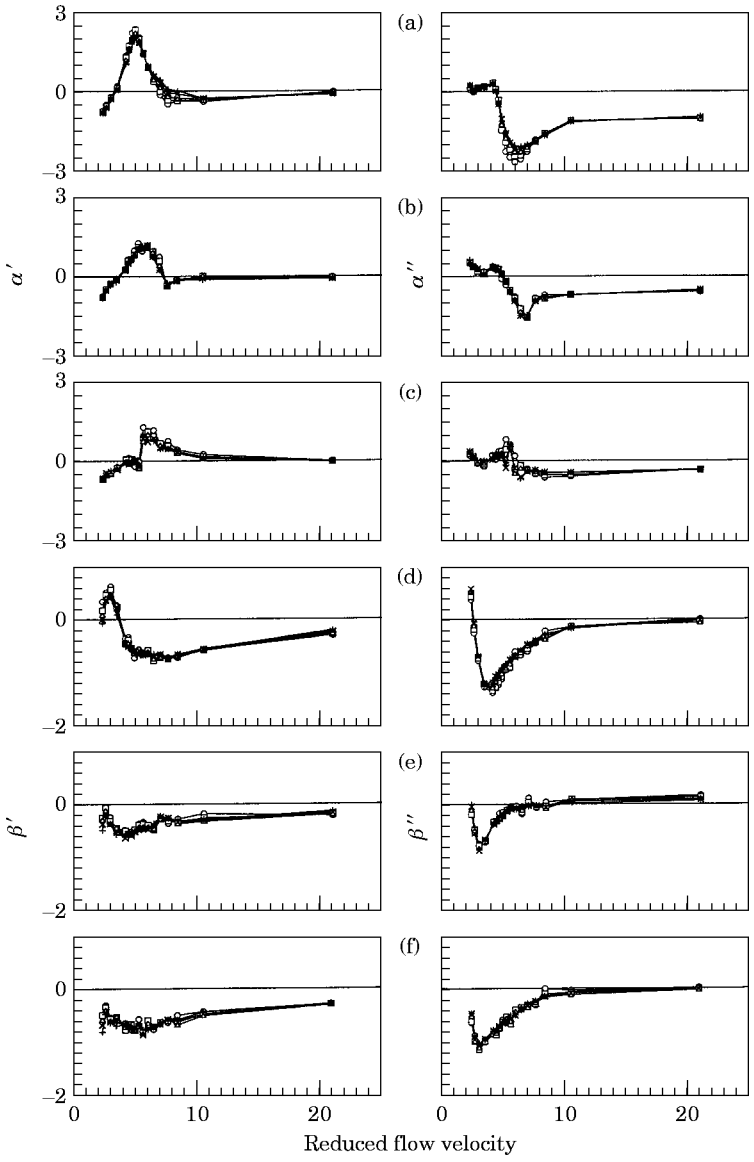

Figure 7. Fluid damping coefficients α' and β' and fluid stiffness coefficients α'' and β'' for tube in downstream position of two tubes in tandem (case c): (a) α' and α'', case c.1; (b) α' and α'', case c.2; (c) α' and α'', case c.3; (d) β' and β'', case c.1; (e) β' and β'', case c.2; (f) β' and β'', case c.3. Excitation amplitudes: –○–, $d/D = 0{\cdot}05$; –□–, $d/D = 0{\cdot}06$; –△–, $d/D = 0{\cdot}07$; –×–, $d/D = 0{\cdot}08$; +, $d/D = 0{\cdot}09$.

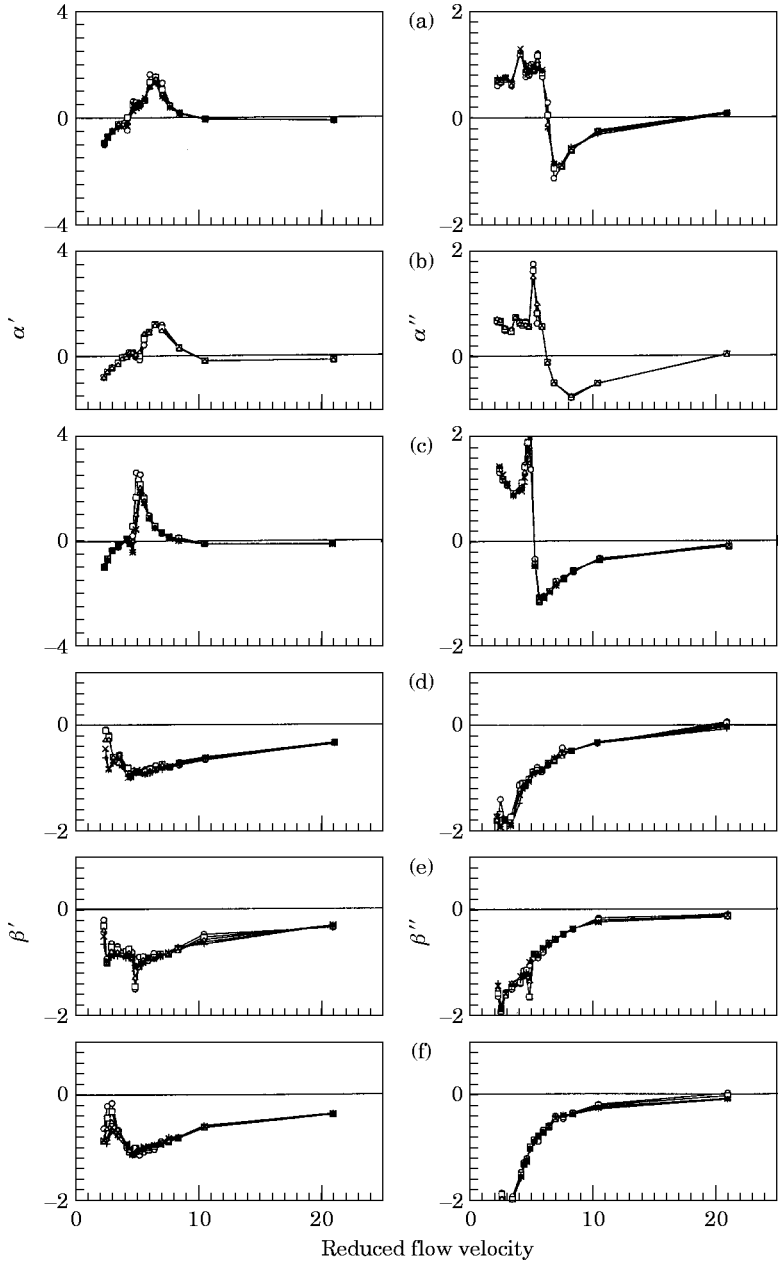

Figure 8. Fluid damping coefficients α' and β' and fluid stiffness coefficients α'' and β'' for a tube in the wake of another tube (case d): (a) α' and α'', case d.1; (b) α' and α'', case d.2; (c) α' and α'', case d.3; (d) β' and β'', case d.1; (e) β' and β'', case d.2; (f) β' and β'', case d.3. (a, c–f): –○–, $d/D = 0{\cdot}05$; –□–, $d/D = 0{\cdot}06$; –△–, $d/D = 0{\cdot}07$; –×–, $d/D = 0{\cdot}08$; +, $d/D = 0{\cdot}09$. (b): –○–, $d/D = 0{\cdot}075$; –□–, $d/D = 0{\cdot}085$; –△, $d/D = 0{\cdot}095$.

test was performed for Ur up to 60). On the other hand, β' is negative for all Ur.

When the tube is in a position that is downstream of another tube, the force coefficients are as shown in Figure 7. α' is positive at lower Ur, whereas β' is

negative only in a small range. As P/D increases, the magnitude of α' decrease and the region of positive α' shifts to larger Ur.

3.2.4. *A tube in the wake of another tube*

The general characteristics of α', α'', β', and β'' shown in Figures 8(a)–8(f), are similar for the tube in three different positions in the wake of the tubes in the upstream position. β' and β'' are negative in the tested reduced flow velocity range. However, α' is positive at the lower reduced flow velocity; its peak value depends on location and can be much larger than the peak value of a single tube.

3.2.5. *Tube row*

The general trend of α' and α'' in cases e.1 (Figures 9 and 10) and e.2 (Figure 11) is similar to the trends observed for a single tube. However, the region of positive

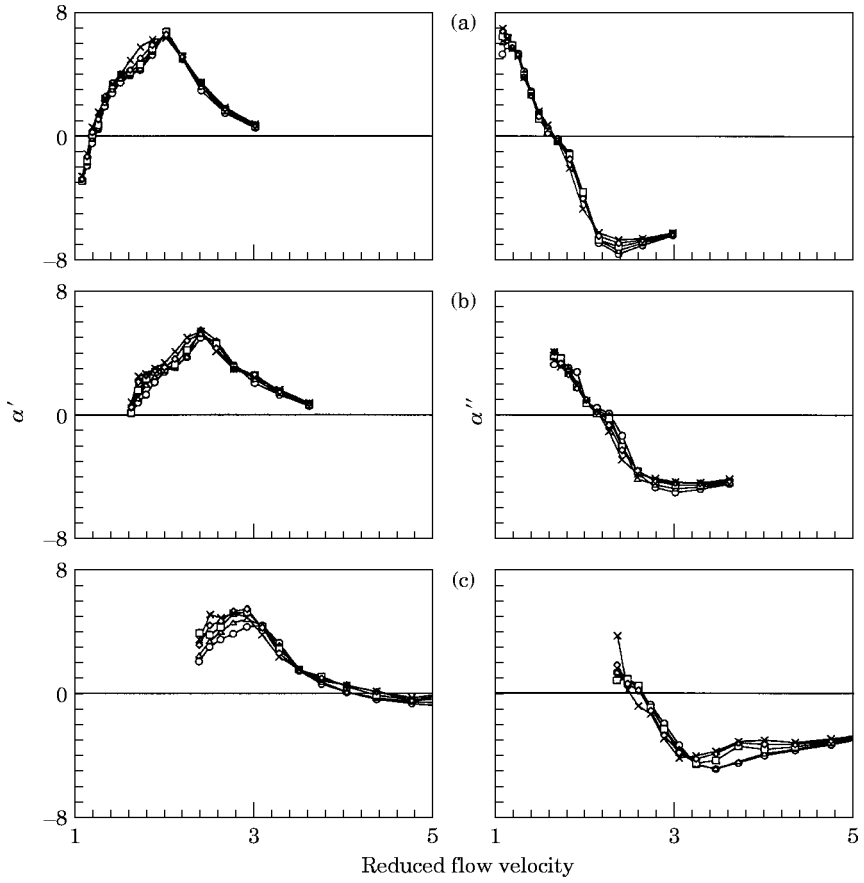

Figure 9. Fluid damping coefficient α' and fluid stiffness coefficient α'' for tube row with $T/D = 1{\cdot}35$ (case e.1.): (a) Re = 1580; –○–, $d = 2{\cdot}3$ mm; –△–, $d = 2{\cdot}1$ mm; –□–, $d = 1{\cdot}9$ mm; –◇–, $d = 1{\cdot}7$ mm; –×–, $d = 1{\cdot}5$ mm. (b) Re = 2310: –○–, $d = 2{\cdot}3$ mm; –△–, $d = 2{\cdot}05$ mm; –□–, $d = 1{\cdot}8$ mm; –◇–, $d = 1{\cdot}55$ mm; –×–, $d = 1{\cdot}3$ mm. (c) Re = 3340: –○–, $d = 2{\cdot}3$ mm; –△–, $d = 2{\cdot}05$ mm; –□–, $d = 1{\cdot}8$ mm; –◇–, $d = 1{\cdot}55$ mm; –×–, $d = 1{\cdot}3$ mm.

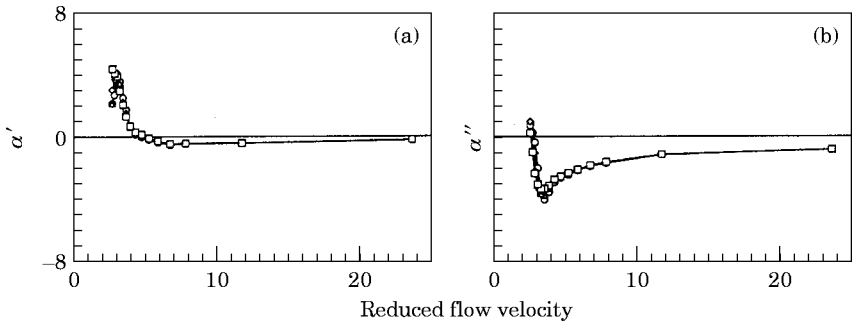

Figure 10. (a) Fluid damping coefficient α' and (b) fluid stiffness coefficient α'' for tube row with $T/D = 1{\cdot}35$ (case e.1) for Re = 3140: –○–, $d = 2{\cdot}4$ mm; –△–, $d = 2$ mm; –◇–, $d = 1{\cdot}6$ mm; –□–, $d = 1{\cdot}2$ mm.

α' for case e.1 is at lower reduced flow velocity. This can be seen clearly from Figure 9. At lower Re, the effects of oscillation amplitude appear to be smaller than those at a larger Re. In case e.2, the pitch-to-diameter ratio is much larger and the general characteristics of α' and α'' are about the same as those of a single tube.

3.2.6. *Triangular array*

The damping coefficients α' and β' shown in Figure 12 show that, in cases f.1 and f.2, when the tube is in the upstream and middle position in the tube array, they are negative at all reduced flow velocity. The only case in which α' becomes positive is at low reduced flow velocity in case f.3, when the tube is in the downstream position. The general trend of α', β' and β'' as a function of reduced flow velocity is similar for the three cases.

3.2.7. *Square arrays*

Figures 13–15 show that fluid force coefficients, α', α'', β' and β'', depend on pitch-to-diameter ratio and tube location. β' is positive for the tube at any location, regardless of pitch-to-diameter ratio. α'' and β'' are similar for the tube at various locations and differing pitch-to-diameter ratio. α' depends on tube location and pitch-to-diamter ratio. When the tube is in the upstream position, α' is negative except at very small Ur; at large Ur, it is always positive. The crossing point from negative to positive values depends on Re, pitch-to-diameter ratio, and tube location. For a fixed Re, the crossing point of α' from negative to positive is the smallest for the tube in the upstream position and largest for the tube in the downstream position. This can be seen clearly from Figure 15(a).

4. FLUID DAMPING CONTROLLED INSTABILITY

Once motion dependent fluid forces are known, the response of the tube can be predicted. As an example, consider a single tube supported by springs. The tube

is subjected to a crossflow uniformly along its length. The equation of motion in the lift direction is

$$m\frac{\mathrm{d}^2u}{\mathrm{d}t^2} + C\frac{\mathrm{d}u}{\mathrm{d}t} + Ku + \frac{\rho\pi D^2}{4}\alpha\frac{\mathrm{d}^2u}{\mathrm{d}t^2} - \frac{\rho U^2}{\omega}\alpha'\frac{\mathrm{d}u}{\mathrm{d}t} - \rho U^2\alpha'' u = \tfrac{1}{2}\rho U^2 D C_L' \cos(\omega_s t), \tag{9}$$

where K is the spring constant, C is the tube damping coefficient, m is the tube mass per unit length, C_L' is the fluctuating lift coefficient, and ω_s is the circular frequency of vortex shedding.

The in-vacuum variables, i.e., natural frequency f_v and modal damping ratio ζ_v, can be calculated from the equation of motion or from an in-vacuum test (practically in air). Let

$$u(z, t) = Dq(t), \qquad Ur = U/fD, \qquad \gamma = \rho\pi D^2/4m, \tag{10}$$

where f is oscillation frequency and U is gap velocity. Substituting equations 10 in equation 9, one obtains

$$\mathrm{d}^2q/\mathrm{d}t^2 + 2\zeta\omega\,\mathrm{d}q/\mathrm{d}t + \omega^2 q = [1/2(1+\gamma\alpha)](\rho U^2 C_L'/m)\cos(\omega_s t), \tag{11}$$

where

$$\omega = \omega_v(1+\gamma C_M)^{-0{\cdot}5},$$

$$\zeta = [\zeta_v/(1+\gamma\alpha)][(1+\gamma C_M)^{0{\cdot}5} - \gamma U r^2\alpha'/2\zeta_v\pi^3], \qquad C_M = \alpha + Ur^2\alpha''/\pi^3. \tag{12}$$

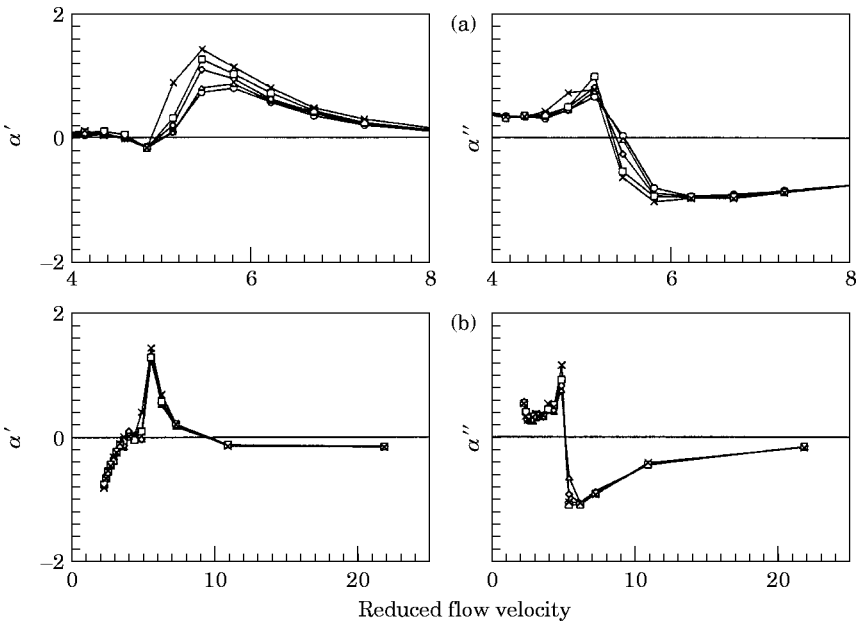

Figure 11. Fluid damping coefficient α' and fluid stiffness coefficient α'' for tube row with $T/D = 2{\cdot}7$ (case e.2) for Re = 2760: −○−, $d = 2{\cdot}8$ mm; −△−, $d = 2{\cdot}4$ mm; −◇−, $d = 2$ mm; −□−, $d = 1{\cdot}6$ mm; −×−, $d = 1{\cdot}2$ mm.

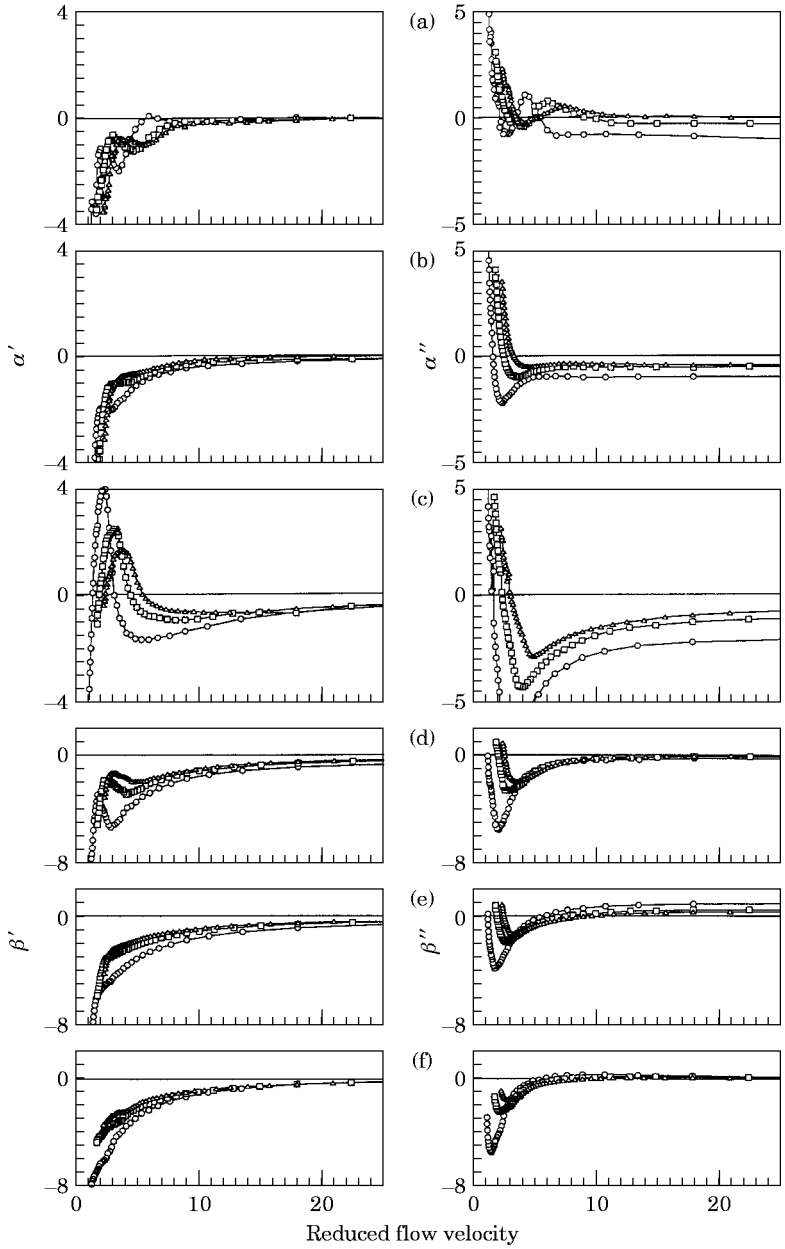

Figure 12. Fluid damping coefficients α' and β' and fluid stiffness coefficients α'' and β'' for triangular array (case f): –○–, Re = 1760; –□–, Re = 2760; –△–, Re = 4010. (a, d) case f.1; (b, e) case f.2, (c, f) case f.3.

Note that ω and ζ are the circular frequency and modal damping ratio, respectively, for the tube in crossflow. C_M is called an added-mass coefficient for the tube in flow; when $Ur = 0$, it is equal to α. When $Ur \neq 0$, C_M depends on Ur as well as on α'', which in turn, depends on Ur and oscillation amplitude.

For motion in the drag direction, equations (11) and (12) are applicable as long as the fluid force coefficients α, α' and α'' are replaced by β, β' and β'' and the

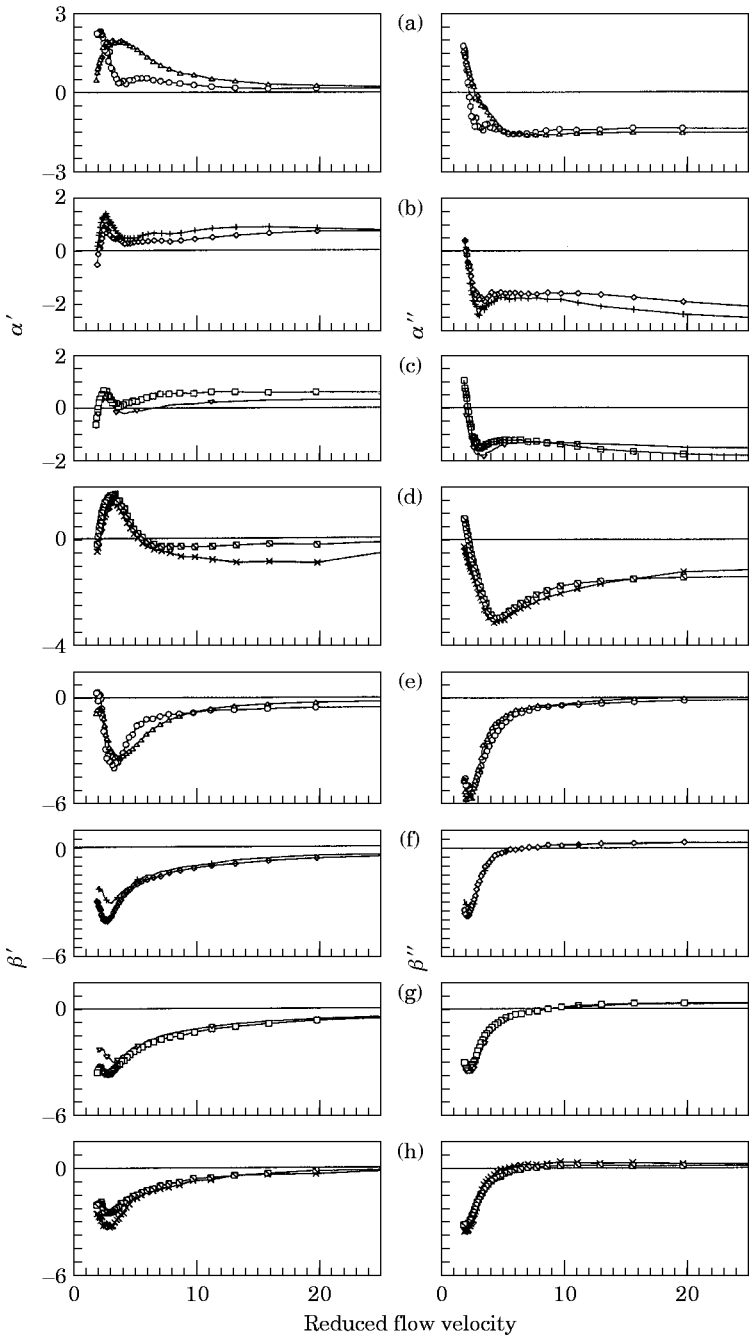

Figure 13. Fluid damping and fluid stiffness coefficients for square tube array with $P/D = 1{\cdot}35$ (case g): (a, e) –○–=case g.1, test 1; –△–=case g.1, test 2; (b, f) –◇–=case g.2, test 1; + =case g.2, test 2; (c, g) –□–=case g.3, test 1; –▽–=case g.3, test 2; (d, h) –×–=case g.4, test 1, –⧅– = case g.4, test 2.

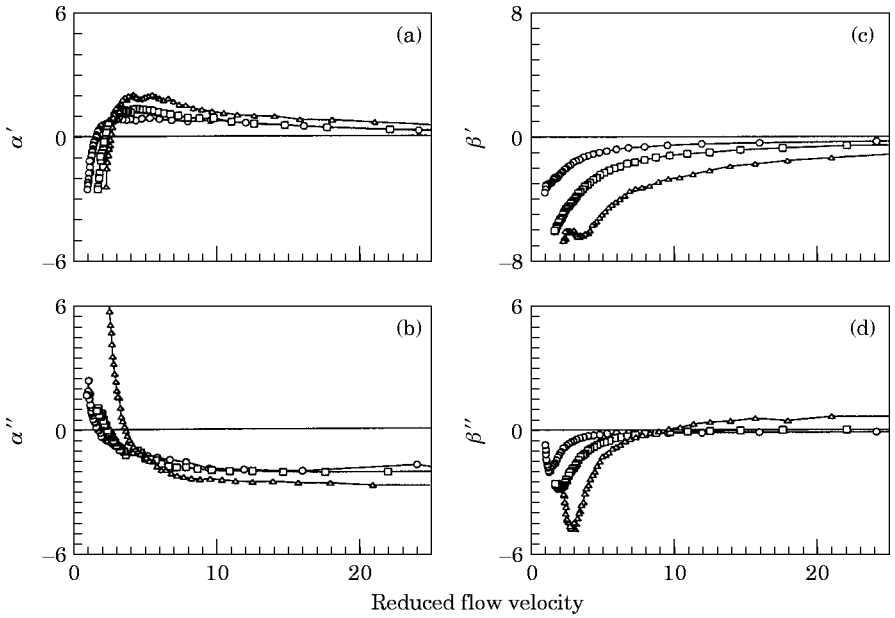

Figure 14. (a) Fluid damping coefficient α', (b) fluid stiffness coefficient α'', (c) fluid damping coefficient β', and (d) fluid stiffness coefficient β'' for square tube array with $P/D = 1{\cdot}42$ (case h): –○–, Re = 1540; –□–, Re = 2810; –△–, Re = 4010.

lift coefficient C_L' and vortex shedding frequency ω_s are replaced by the drag coefficient C_D' and $2\omega_s$, respectively. The system response due to vortex shedding and other excitation can be obtained by solving equation (11). Note that inasmuch as the fluid force coefficients α' and α'' are a function of Ur, the natural frequency ω and modal damping ratio ζ are a function of the reduced flow velocity Ur. The unsteady flow theory can form the basis for calculating a complete response that is due to flow. The calculation will require an iteration technique.

When modal damping becomes negative, the tube becomes dynamically unstable and high amplitude oscillations develop. As the oscillation amplitude increases, other non-linear effects may become important and the system may be stabilized. The critical flow velocity of dynamic instability can be calculated from

$$\zeta = 0. \tag{13}$$

From equations (12) and (13), the critical reduced flow velocity at which the modal damping ratio is zero can be calculated from

$$Ur = 4\sqrt{2\pi}(\delta/\alpha')^{0{\cdot}5}[(\delta/\pi^2)(\alpha''/\alpha') \pm \sqrt{((\delta/\pi^3)(\gamma\alpha''/\alpha'))^2 + (1+\gamma\alpha)/4}]^{0{\cdot}5}, \tag{14}$$

where δ is a mass-damping parameter ($\delta = 2\pi\zeta_v m/\rho D^2$). This is the critical flow velocity for fluidelastic instability in the lift direction. Similarly, the critical flow velocity for motion in the drag direction is

$$Ur = 4\sqrt{2\pi}(\delta/\beta')^{0{\cdot}5}[(\delta/\pi^2)(\beta''/\beta') - \sqrt{((\delta/\pi^3)\gamma\beta''/\beta')^2 + (1+\gamma\beta)/4}]^{0{\cdot}5}. \tag{15}$$

The critical flow velocity for fluid damping controlled instability can be calculated from equations (14) and (15). Because α', β, α'' and β'' depend on Ur, the calculation requires an iteration process.

5. DISCUSSIONS AND NUMERICAL EXAMPLES

The modal damping ratio given in equation (12) shows that it consists of two parts, tube damping and fluid damping. Tube damping is always positive whereas fluid damping may be positive or negative. To make the total damping ratio negative, α' or β' must be positive. Table 1, based on the fluid force coefficients,

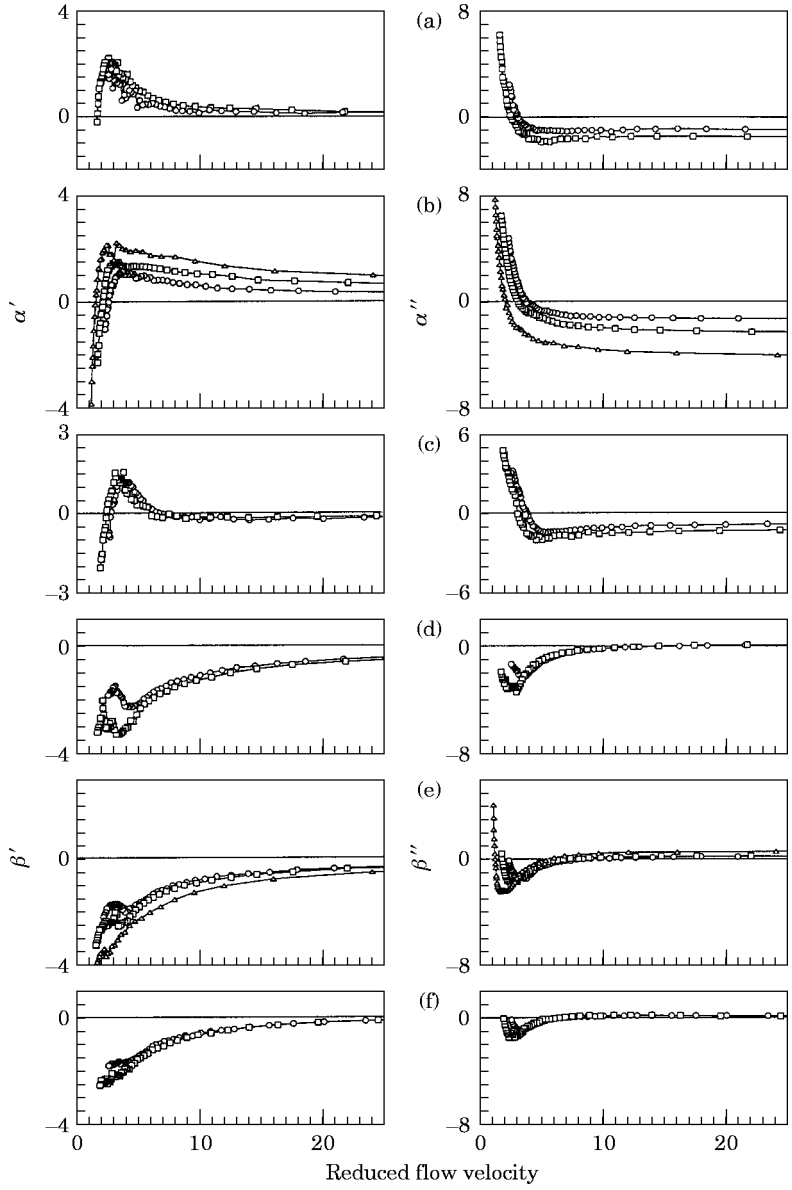

Figure 15. Fluid damping coefficients α' and β' and fluid stiffness coefficients α'' and β'' for square array with $P/D = 1{\cdot}46$ (case i): (a, d) case i.1, –○–, Re = 4140; –□–, Re = 2780; (b, e) case i.2, –○–, Re = 4010, –□–, Re = 2810; –△–, Re = 1540; (c, f) case i.3, –○–, Re = 4490; –□–, Re = 3130.

TABLE 1

Regions with positive α' and β' in which fluidelastic instability may occur

Cases		Pitch-to-diameter ratio (P/D)	Lift direction	Drag direction
a	(single tube)	–	$5 < Ur < 11$	Not measured
b	(two tubes normal to flow)	1·35 (T/D)	$2 < Ur < 6$	None
c.1	(two tubes in tandem) upstream tube	1·35	$7 < Ur$	None
c.1	(two tubes in tandem) downstream tube	1·35	$3{\cdot}5 < Ur < 8$	$2{\cdot}2 < Ur < 3{\cdot}6$
c.2	(two tubes in tandem) downstream tube	2·70	$3{\cdot}6 < Ur < 7{\cdot}4$	None
c.3	(two tubes in tandem) downstream tube	4·05	$5{\cdot}3 < Ur < 20$	None
d.1	(a tube in the wake of another tube)	2·7 1·35 (T/D)	$4{\cdot}2 < Ur < 10$	None
d.2	(a tube in the wake of another tube)	4·05 1·35 (T/D)	$5{\cdot}2 < Ur < 9{\cdot}5$	None
d.3	(a tube in the wake of another tube)	4·05 2·7 (T/D)	$4{\cdot}7 < Ur < 9{\cdot}3$	None
e.1	(tube row)	1·35 (T/D)	$1{\cdot}1 < Ur < 4{\cdot}0$	None
e.2	(tube row)	2·70 (T/D)	$5 < Ur < 9{\cdot}5$	None
f.1	(triangular array) upstream tube	1·35	$Ur > 25$	None
f.2	(triangular array) middle tube array	1·35	None	None
f.3	(triangular array) downstream tube	1·35	$1{\cdot}5 < Ur < 5{\cdot}5$	$Ur > 30$ (Re = 1760) $Ur > 50$ (Re = 2760) $Ur > 62$ (Re = 4010)
g.1	(square array) upstream tube	1·35	$1{\cdot}5 < Ur$	None
g.2	(square array) second row of tubes	1·35	$2{\cdot}0 < Ur$	None
g.3	(square array) second row from downstream tube	1·35	$2{\cdot}0 < Ur$	None
g.4	(square array) downstream tube	1·35	$2 < Ur < 6$	None
h	(square array) middle of tube array	1·42	$1{\cdot}5 < Ur$	None
i.1	(square array) upstream tube	1·46	$1{\cdot}7 < Ur$	None
i.2	(square array) middle of tube array	1·46	$2{\cdot}1 < Ur$	None
i.3	(square array) downstream tube	1·46	$3{\cdot}1 < Ur < 7$	None

is a summary of the potential instability regions. From Table 1, several conclusions are noted:

(1) The motion in the drag direction is much more stable than that in the lift direction; practically, it will not become unstable by fluid damping controlled instability in the drag direction for various tube arrays.

(2) For a triangular array, fluid damping controlled instability is not possible for the tube in the upstream position and the tube in the middle of tube array because the fluid damping coefficients α' and β' are negative.

(3) For the tube in the upstream position of two tubes in tandem and the tube in the upstream position or in the middle of a square tube array, once the reduced flow velocity reaches a certain value, the damping coefficient α' becomes positive.

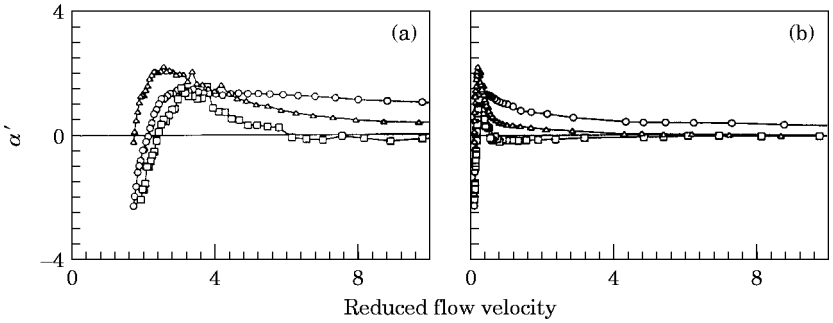

Figure 16. Fluid damping coefficient α' at different positions for square array with $P/D = 1{\cdot}46$: –△–, case i.1, Re = 2780; –○–, case i.2, Re = 2810; –□–, case i.3, Re = 3130.

The effects of tube position, tube pitch, and the tube in the downstream position on fluid-damping coefficient α'' are considered in detail.

5.1. TUBE LOCATION

Fluid force coefficient α' in a square array ($P/D = 1{\cdot}46$) depends on the position of the tube. For example, Figure 16 shows α' for a tube in an upstream, a middle, and a downstream position in a tube array. When Ur reaches a certain value, α' becomes positive. The point at which α' changes its sign depends on tube location. At high Ur, the value of α' for the middle tube is positive for all large Ur whereas for the upstream and downstream tubes, the values of α' become very small and then negative again. Based on α', it can be seen that, in a square array, first the upstream tube will become unstable, then the middle tube, and finally the downstream tube. This was noticed in an earlier experiment with a square array [17, 18]. For the middle tube, the instability is sustained for all Ur. The effect of

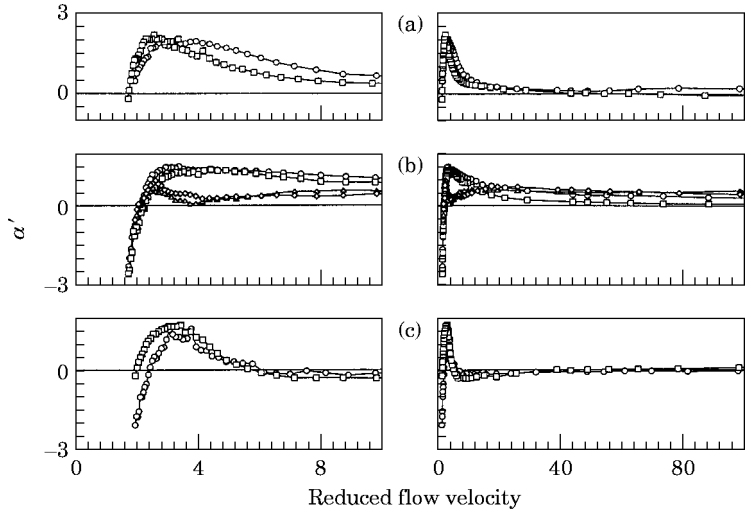

Figure 17. Fluid damping coefficient α' for square array: (a) –○–, case g.1, Re = 2510; –□–, case i.1, Re = 2870; (b) –◇–, case g.2, Re = 2510; –△–, case g.3, Re = 2510; –○–, case h, Re = 2810; –□–, case i.2, Re = 2810; (c) –□–, case g.4, Re = 2510; –○–, case i.3, Re = 2810.

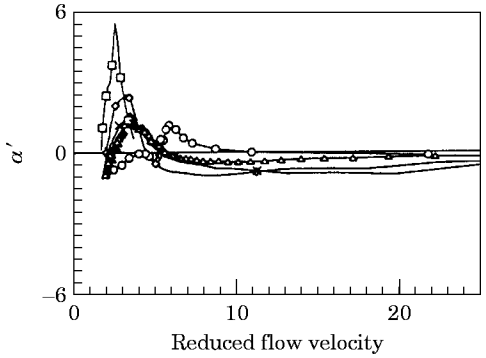

Figure 18. Fluid damping coefficient α' of tube in various arrays and positions for pitch-to-diameter ratio fo 1·35 and various Re: –○–, single tube, Re = 2760; –△–, two tubes normal to flow, Re = 2830; –□–, tube row, Re = 2310; –◇–, triangular array, downstream, Re = 2760; –×–, square array, downstream, Re = 2510.

tube location for triangular arrays is different; the downstream tube can become unstable.

5.2. TUBE PITCH

Fluid force coefficients depend on pitch-to-diameter ratio. Figure 17 shows α' for three values of P/D (1·35, 1·42, and 1·46) for a square array. For tubes in the upstream and middle positions, the crossing point of α' is almost independent of P/D, whereas for the tube in the downstream position, the crossing point is approximately the same as that of a tube row [12]. The value of α' at high Ur for the tube in the upstream and middle positions does depend on P/D. For the downstream tube, the effect is much smaller. This is consistent with the previous data on fluidelastic instability of square arrays [17].

5.3. DOWNSTREAM TUBE

Figure 18 shows α' for various tube arrays with $P/D = 1{\cdot}35$. In all cases, at lower Ur corresponding to the vortex shedding region, α' is positive. The location and

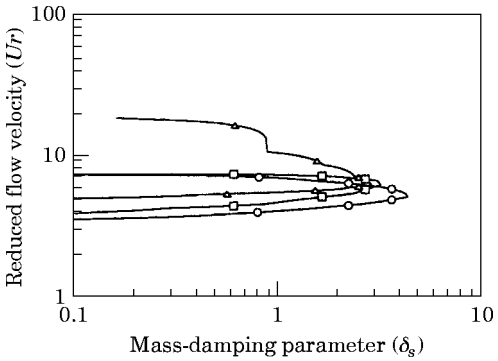

Figure 19. Fluid damping controlled instability boundaries for downstream tube in two-tubes-in-tandem array: –○–, case c.1, $P/D = 1{\cdot}35$; –□–, case c.2, $P/D = 2{\cdot}7$; –△–, case c.3, $P/D = 4{\cdot}05$.

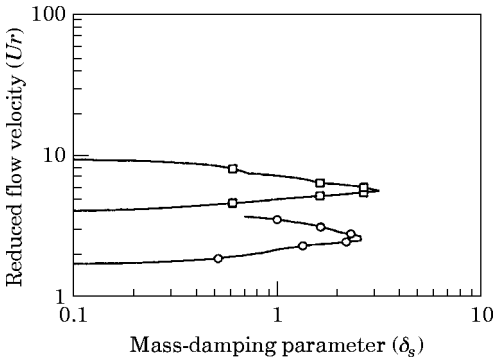

Figure 20. Fluid damping controlled instability boundaries for tube in tube row array: –○–, case e.1, Re = 2310, $T/D = 1{\cdot}35$; –□–, case e.2, Re = 3140, $T/D = 2{\cdot}7$.

the range depend on tube array. The single tube occurs at higher Ur while tube arrays occurs at lower Ur. The peak value of α' is largest for a tube row, smaller for a triangular tube array, and finally, for a square array and two tubes normal to flow, it is smallest. It is also noted that the first crossing points of α' for all tube arrays are very close to each other. Another characteristic is that the crossing point of α' from negative to positive occurs at lower Ur for lower Re. For two tubes in tandem, a tube row, and square arrays, the crossing point of α' from negative to positive also occurs at lower Ur for lower Re.

For two tubes in tandem, a tube row, triangular array, and square arrays, the stability boundaries for fluid damping controlled instability as a function of mass-damping parameter, δ_s, are shown in Figures 19–23. Figure 19 shows that, for two tubes in tandem, fluid damping controlled instability occurs at lower δ_s. The lower boundaries vary with P/D but change slowly with δ_s. When P/D is smaller, the critical flow velocity is also lower.

When the array is a tube row (Figure 20), the general behavior is similar to that of two tubes in tandem. Fluid damping controlled instability occurs at lower δ_s. The lowest critical flow velocity increases with tube T/D.

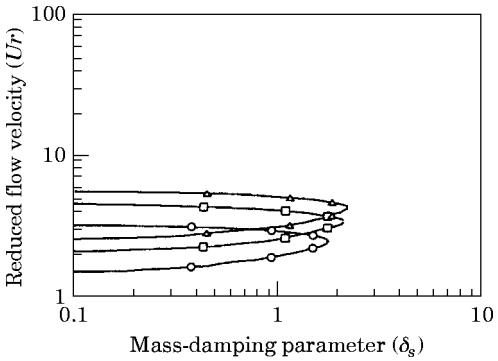

Figure 21. Fluid damping controlled instability boundaries for downstream tube in triangular array, case f.3, $P/D = 1{\cdot}35$: –○–, Re = 1760; –□–, Re = 2760; –△–, Re = 4010.

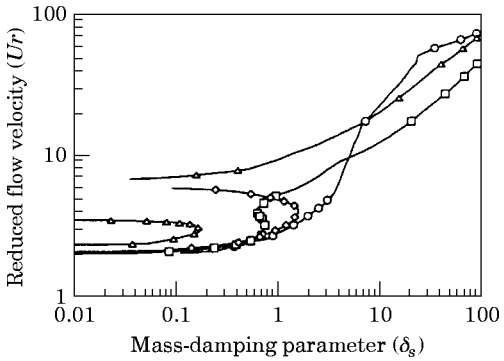

Figure 22. Fluid damping controlled instability boundaries for square array, $P/D = 1{\cdot}35$: –○–, case g.1, upstream tube; –□–, case g.2, second row tube; –△–, case g.3, third row tube; –◇–, case g.4, downstream tube.

In the case of a triangular array (Figure 21), fluid damping controlled instability occurs when δ_s is less than ≈ 2. The instability region depends on Re. As Re increases, the region moves upward; this means that the critical flow velocity is greater. In this case, the size of the instability region is almost independent of Re.

For square arrays (Figures 22 and 23), fluid damping controlled instability can occur at various values of δ_s, depending on the location of the tube. Except for the downstream tube, which is similar to a downstream tube in a triangular array, fluid damping controlled instability can occur in the whole range of δ_s. For a tube in the second and third rows, there is a sudden increase of the critical flow velocity at a specific δ_s, $\approx 0{\cdot}75$ and $0{\cdot}18$ for tubes in the second and third rows, respectively.

6. CLOSING REMARKS

In summary, a large data base for fluid force coefficients is presented in this paper. These data provide the needed information to predict tube response and evaluation of tube response in different tube arrays, different locations, and different flow conditions. No such comprehensive data base is available in the literature.

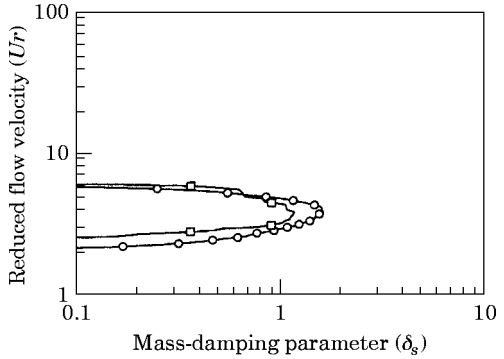

Figure 23. Fluid damping controlled instability boundaries for square array, downstream tube: –○–, case g.4, $P/D = 1{\cdot}35$; –□–, case i.3, $P/D = 1{\cdot}46$.

This paper describes a direct measurement technique for fluid damping and fluid stiffness that adequately characterizes the fluid effects of fluid damping controlled instability for various tube arrays. The critical components of fluid forces are described by α' and β'. Once these two fluid force coefficients are measured, they can be used in practical applications. Similar data have been used successfully to predict lock-in resonance of a single tube in crossflow [13].

A change in response frequency is determined by fluid stiffness and mass ratio, whereas stability depends on fluid damping. In some regions of reduced flow velocity, fluid damping may be negative when α' and β' are positive; this means that the energy of the fluid is being pumped into the structural system. Fluid damping controlled instability of a single flexible tube in a tube array can be determined immediately from the sign of α' and β'.

α' and β' depend on many system parameters: Re, tube pitch, tube pattern, reduced flow velocity, and oscillation amplitude (from 2%–14% of tube diameter). Some general conclusions can be reached from the fluid-force coefficients α' and β' presented in this paper.

Fluid damping controlled instability is most likely to be associated with the motion in the lift direction because in many cases, α' is positive while β' is negative.

When the reduced flow velocity is small, say $Ur < 10$, α' and β' depend on Re. At large Ur, Re has little effect on α' and β'. In the region of Ur where α' is positive, the point at which α' changes from negative to positive or positive to negative shifts to larger Ur as Re increases.

α' and β' may depend on the pitch-to-diameter ratio. For square arrays, the effect of P/D is very small. This means that, for square tube arrays with differing P/D, the critical flow velocities for damping controlled instability are approximately the same and a single stability criterion can be used for various P/D values. On the other hand, for tube rows and triangular arrays, different criteria must be used for different P/D.

In square tube arrays, the most unstable position is that of the tube in the upstream position in the array and the most stable position is that of the downstream tube in the array. On the other hand in the triangular tube array, the upstream tube and the tube in the middle of tube array are stable.

The stability of the downstream tube in various tube arrays is very similar to that of a single tube. This is attributed to the vortex shedding associated with the downstream tube. In all cases, there is a limited range of Ur in which the tube is subjected to fluid-damping controlled instability.

For fluid damping controlled instability, the interaction effect associated with the motion of the surrounding tubes is less significant. This means that the critical flow velocity of a single flexible tube does not differ very much from that of a group of flexible tubes. On the other hand, the interaction of multiple-tube motions is a necessary condition for fluid stiffness controlled instability.

On the basis of unsteady flow theory, fluidelastic instability can be defined specifically. Because of fluid damping, when the resultant modal damping ratio becomes zero, the tube is subjected to fluidelastic instability regardless of the source of fluid damping. On the other hand, when the modal damping ratio is >0

and the tube oscillation amplitudes are large because of other excitation sources (such as vortex shedding), one has forced excitation. For example, lock-in resonance due to vortex sheding may be in the fluidelastic instability region or forced excitation, depending on *Ur* and other parameters.

In summary, based on the present results, one concludes that unsteady flow theory is a simple model that can be used to predict tube response. In addition, the theory points out the role of fluidelastic instability associated with other excitation mechanisms. For example, vortex-induced vibration is a coupled forced vibration and also fluidelastic instability when the vortex shedding frequency is close to the natural frequency of a cylinder. Unsteady flow theory can be used to examine detailed characteristics in the instability regions as well as forced responses due to other excitation sources.

ACKNOWLEDGMENT

This work was funded by the Electric Power Research Institute under an agreement with the U.S. Department of Energy, Contract Agreement 31-109-Eng-38-85989.

REFERENCES

1. S. S. CHEN 1987 *Flow-Induced Vibration of Circular Cylindrical Structures*. New York: Hemisphere Publishing.
2. S. S. CHEN 1987 *Journal of Fluids and Structures* **1**, 35–53. A general theory for dynamic instability of tube arrays in crossflow.
3. S. J. PRICE 1993 *Technology for the '90s, A Decade of Progress*. New York: ASME, 711–773. Theoretical models of fluidelastic instability for cylinder arrays subjected to cross flow.
4. H. J. CONNORS 1970 *Flow-Induced Vibration in Heat Exchangers* (D. D. Reiff, editor), 42–56, New York: ASME. Fluidelastic vibration of tube arrays excited by cross flow.
5. S. S. CHEN 1983 *Journal of Vibration, Acoustics, Stress and Reliability in Design* **105**, 51–58. Instability mechanisms and stability criteria of a group of circular cylinders subjected to cross flow: part I, theory.
6. S. J. PRICE, B. MARK and M. P. PAIDOUSSIS 1986 *Journal of Pressure Vessel Technology* **108**, 62–72. An experimental stability analysis of a single flexible cylinder positioned in an array of rigid cylinders and subject to cross-flow.
7. S. J. PRICE and M. P. PAIDOUSSIS 1987 *Proceedings of the International Conference on Flow-Induced Vibrations, Bowness-on-Windermere, UK*. BHRA, the Fluid Engineering Center, Cranfield, Bedford, England. 51–63. The flow-induced response of a single flexible cylinder in an in-line array of rigid cylinders.
8. S. S. CHEN 1983 *Journal of Vibration, Acoustics, Stress and Reliability in Design* **105**, 253–260. Instability mechanisms and stability criteria of a group of circular cylinders subjected to cross flow: part II, numerical results and discussions.
9. H. TANAKA 1980 *Nihon Kikai Gakkai Ronbunshu* (*Japan Society of Mechanical Engineering*) Section B **46**, 1398–1407. Study on fluidelastic vibration of tube bundle.
10. H. TANAKA and S. TAKAHARA 1981 *Journal of Sound and Vibration* **77**, 19–37. Fluid elastic vibration of tube array in cross flow.
11. H. TANAKA, S. TAKAHARA and K. OHTA 1982 *Journal of Pressure Vessel Technology* **104**, 168–174. Flow-induced vibration of tube arrays with various pitch-to-diameter ratios.

12. S. S. CHEN, S. ZHU and J. A. JENDRZEJCZYK 1994 *Journal of Pressure Vessel Technology* **116**, 370–383. Fluid damping and fluid stiffness of a tube row in crossflow.
13. S. S. CHEN, S. ZHU and Y. CAI 1995 *Journal of Sound and Vibration* **184**, 73–92. An unsteady flow theory for vortex-induced vibration.
14. S. S. CHEN, Y. CAI and S. ZHU 1996 *Journal of Offshore Mechanics & Arctic Engineering* **118**, 253–258. Flow-induced vibration of tubes in crossflow.
15. S. ZHU, Y. CAI and S. S. CHEN 1995 *Journal of Engineering Mechanics* **121**, 1003–1005. Experimental fluid-force coefficients for wake-induced cylinder vibration.
16. S. ZHU, S. S. CHEN and Y. CAI 1997 *Journal of Pressure Vessel Technology* **119**, 142–149. Vibration and stability of two tubes in crossflow.
17. S. S. CHEN and J. A. JENDRZEJCZYK 1981 *Journal of Sound and Vibration* **78**, 355–381. Experiments on fluid elastic instability in tube banks subjected to liquid cross flow.
18. S. S. CHEN 1984 *Journal of Sound and Vibration* **93**, 439–455. Guidelines for the instability flow velocity of tube arrays in crossflow.